electronics

Article

Field Programmable Analog Array Based Non-Integer Filter Designs

Alexandros Pagidas [1], Costas Psychalinos [1,*] and Ahmed S. Elwakil [2,3,4]

1 Department of Physics, Electronics Laboratory, University of Patras, 26504 Patras, Greece
2 Department of Electrical Engineering, University of Sharjah, Sharjah P.O. Box 27272, United Arab Emirates; elwakil@ieee.org
3 Nanoelectronics Integrated Systems Center (NISC), Nile University, Giza 12677, Egypt
4 Department of Electrical and Software Engineering, University of Calgary, Calgary, AB T2N 1N4, Canada
* Correspondence: cpsychal@upatras.gr

Abstract: The approximation of the frequency behavior of fractional-order, power-law, and double-order filters can be performed by the same rational integer-order transfer function. This can be achieved through the utilization of a curve fitting based approximation. Moreover, their implementation can be performed by the same core, by only changing the corresponding time constants and scaling factors. The aforementioned findings are experimentally verified using a Field Programmable Analog Array device.

Keywords: non-integer order filters; power-law filters; fractional-order filters; multi-feedback structures; curve fitting approximation; Field Programmable Analog Arrays

check for updates

Citation: Pagidas, A.; Psychalinos, C.; Elwakil, A.S. Field Programmable Analog Array Based Non-Integer Filter Designs. *Electronics* **2023**, *12*, 3427. https://doi.org/10.3390/electronics12163427

Academic Editor: Fábio Passos

Received: 12 July 2023
Revised: 8 August 2023
Accepted: 11 August 2023
Published: 13 August 2023

1. Introduction

Non-integer order filters can be categorized as follows: (a) fractional-order (FO) filters, where the Laplacian operator is raised to a (non-integer) power, (b) power-law (PL) filters, where, instead of employing non-integer forms of the Laplacian operator, the associated integer-order transfer function (also known as the mother function) is raised to a power, and (c) double-order (DO) filters, which combine the employment of the fractional Laplacian operator and of the whole transfer function raised to a power. All these types of filters offer design flexibility because of the extra degree(s) of freedom caused by the non-integer order(s), which appear in their transfer functions. These include the scaling of the time constants and the adjustment of the slope of the gain during the transition from the pass-band to the stop-band of the filter [1].

A significant research effort has been devoted to realizing FO, PL, and DO filters, in which various types of active elements have been utilized, including Operational Amplifiers (Op Amps), Current Conveyors (CCIIs), Current Feedback Operational Amplifiers (CFOAs) etc. [2–9]. These solutions do not offer programmability and, taking into account the nowadays deamand for having available re-configurable structures, programmable filters are preferable. In [10], FO filters were implemented and their programmability was achieved using a Field Programmable Analog Array (FPAA) device. This device has also been used in [11] for implementation of PL filters. In addition, a comparison of the behavior of FO and PL filters, in terms of the realized cut-off frequency, was carried out in that work. A programmable DO filter structure was introduced in [12], where the transconductance parameter of the Operational Transconductance Amplifiers (OTAs) was employed to achieve adjustable frequency characteristics. This type of active element was also employed in [13] for implementation of FO, and in [14] for implementation of PL filters.

The main contributions made in this work are the following: (a) all possible versions of non-integer order filters (i.e., FO, PL, and DO) are considered and studied concerning the effect of the location of the half-power frequency with regards to the pole frequency,

(b) a common procedure for obtaining the approximation transfer function, independently from the type and the order of the filter, is employed, through the deployment of a curve fitting based approximation, and (c) an FPAA based versatile implementation, which is capable of realizing all the aforementioned types of filter functions without any change of the structure, is performed.

The work is organized as follows. The comparative study between the types of non-integer filter functions is performed in Section 2, and the problem of the approximation of their transfer functions by rational integer-order functions is discussed in Section 3. The implementation of the generalized filter is demonstrated in Section 4, where the obtained experimental results are also provided.

2. Non-Integer Order Filters

2.1. Low-Pass Filters

Starting from the conventional (i.e., integer-order) low-pass filter (LPF), with pole frequency ω_0 described by (1):

$$H_{LP}(s) = \frac{\omega_0}{s+\omega_0}, \tag{1}$$

its gain and phase responses are given by (2) and (3) as:

$$|H_{LP}(\omega)| = \frac{1}{\sqrt{\left(\frac{\omega}{\omega_0}\right)^2 + 1}}, \tag{2}$$

$$\angle H_{LP}(\omega) = -\tan^{-1}\left(\frac{\omega}{\omega_0}\right). \tag{3}$$

The half-power frequency (ω_h), also known as -3 dB frequency, is equal to the pole frequency ($\omega_h = \omega_0$), while the phase at this frequency becomes equal to $-\pi/4$. The slope of the transition from the pass-band of the filter to the stop-band is fixed and equal to -20 dB/dec.

The corresponding fractional-order low-pass filter (FO-LPF) is described by the transfer function in (4):

$$H_{FOLP}(s) = \frac{\omega_o^{\alpha}}{s^{\alpha}+\omega_0^{\alpha}}, \tag{4}$$

with $0 < \alpha < 1$ being the order of the filter. Setting $s^{\alpha} = \omega^{\alpha}[\cos(0.5\pi\alpha) + j\sin(0.5\pi\alpha)]$ in (4), its magnitude and phase responses are provided by (5) and (6):

$$|H_{FOLP}(\omega)| = \frac{1}{\sqrt{\left(\frac{\omega}{\omega_0}\right)^{2\alpha} + 2\left(\frac{\omega}{\omega_0}\right)^{\alpha}\cos(\frac{\alpha\pi}{2}) + 1}}, \tag{5}$$

$$\angle H_{FOLP}(\omega) = -\tan^{-1}\left[\frac{\left(\frac{\omega}{\omega_o}\right)^{\alpha}\sin(\frac{\alpha\pi}{2})}{\left(\frac{\omega}{\omega_0}\right)^{\alpha}\cos(\frac{\alpha\pi}{2}) + 1}\right]. \tag{6}$$

The associated half-power frequency, as well as the phase at this frequency, are given by (7) and (8) respectively:

$$\frac{\omega_{h,FOLP}}{\omega_0} = \left[\sqrt{1+\cos^2(\frac{\alpha\pi}{2})} - \cos(\frac{\alpha\pi}{2})\right]^{1/\alpha}, \tag{7}$$

$$\angle H_{FOLP}(\omega_{h,FOLP}) = -\tan^{-1}\left[\frac{\sin(\frac{\alpha\pi}{2})}{2\cos(\frac{\alpha\pi}{2}) + \sqrt{1+\cos^2(\frac{\alpha\pi}{2})}}\right]. \tag{8}$$

It must be mentioned at this point that the half-power and the pole frequencies are different, and their relative distance is determined by the order of the filter. In addition, the slope of the transition from the pass-band of the filter to the stop-band is variable because it is given by the formula $-20 \cdot \alpha$ dB/dec.

The power-law low-pass filter (PL-LPF) is derived by raising the transfer function in (1) to a non-integer power $0 < \beta < 1$; therefore,

$$H_{PLLP}(s) = \left(\frac{\omega_0}{s+\omega_0}\right)^{\beta}. \tag{9}$$

Setting $s = j\omega$ in (9), the expressions of the gain and phase responses, as well as of the half-power frequency and its associated phase, are summarized in (10)–(13):

$$|H_{PLLP}(\omega)| = \frac{1}{\left[\left(\frac{\omega}{\omega_0}\right)^2 + 1\right]^{\beta/2}}, \tag{10}$$

$$\angle H_{PLLP}(\omega) = -\beta \cdot \tan^{-1}\left(\frac{\omega}{\omega_0}\right), \tag{11}$$

$$\frac{\omega_{h,PLLP}}{\omega_0} = \sqrt{2^{1/\beta} - 1}, \tag{12}$$

$$\angle H_{PLLP}(\omega_{h,PLLP}) = -\beta \cdot \tan^{-1}\left(\sqrt{2^{1/\beta} - 1}\right). \tag{13}$$

The distance between the half-power frequencies is determined by the order of the filter and this is true for the gradient between the pass-band and the stop-band of the filter, which is equal to $-20 \cdot \beta$ dB/dec.

Generalizing the above, the double-order low-pass filer is described by (14):

$$H_{DOLP}(s) = \left(\frac{\omega_0^{\alpha}}{s^{\alpha}+\omega_0^{\alpha}}\right)^{\beta}, \tag{14}$$

and, therefore, the derived expressions of the gain and phase responses are

$$|H_{DOLP}(\omega)| = \frac{1}{\left[\left(\frac{\omega}{\omega_0}\right)^{2\alpha} + 2\left(\frac{\omega}{\omega_0}\right)^{\alpha}\cos(\frac{\alpha\pi}{2}) + 1\right]^{\beta/2}}, \tag{15}$$

$$\angle H_{DOLP}(\omega) = -\beta \cdot \tan^{-1}\left[\frac{\left(\frac{\omega}{\omega_0}\right)^{\alpha}\sin(\frac{\alpha\pi}{2})}{\left(\frac{\omega}{\omega_0}\right)^{\alpha}\cos(\frac{\alpha\pi}{2}) + 1}\right]. \tag{16}$$

Using (15) and (16), the half-power of the filter is given by (17):

$$\frac{\omega_{h,DOLP}}{\omega_0} = \left[\sqrt{2^{1/\beta} - \sin^2(\frac{\alpha\pi}{2})} - \cos(\frac{\alpha\pi}{2})\right]^{1/\alpha}, \tag{17}$$

while the phase at this frequency is given by (18):

$$\angle H_{DOLP}(\omega_{h,DOLP}) = -\beta \cdot \tan^{-1}\left[\frac{\left(2^{1/\beta}-1\right)\sin\left(\frac{\alpha\pi}{2}\right)}{2^{1/\beta}\cos\left(\frac{\alpha\pi}{2}\right)+\sqrt{2^{1/\beta}-\sin^2\left(\frac{\alpha\pi}{2}\right)}}\right]. \tag{18}$$

The variation in the half-power frequency with the order of an FO-LPF (α) and of a PL-LPF (β), calculated using (7) and (12), respectively, are plotted in Figure 1a.

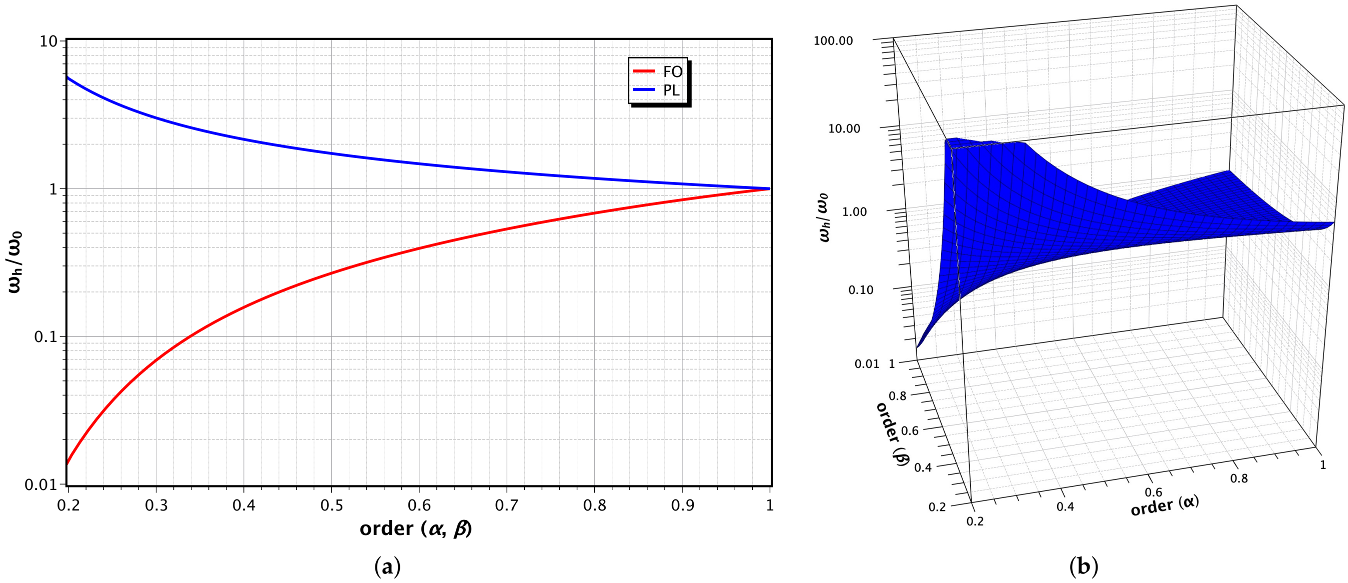

Figure 1. Variation in the half-power frequency of (**a**) FO-LPF and PL-LPF as a function of the order α, and (**b**) DO-LPF as a function of the orders (α, β).

The main difference between the fractional-order and power-law filters is the relative position of the half-power frequencies ω_h with respect to the pole frequency ω_0. As the order decreases with regards to its maximum value (which is equal to one), the cut-off frequency of the fractional-order filter becomes smaller than that which corresponds to the maximum value of the order (equal to ω_0). The opposite situation holds in the case of the power-law filter.

In the case of DO-LPF, the orders α and β can be considered as two degrees of freedom, and the relationship between the cut-off frequency and the orders of the filter can be illustrated in a three-dimensional graph, as shown in Figure 1b. By changing the orders α and β, the cut-off frequency can be smaller or greater than the characteristic frequency ω_0. According to (17), for values of orders near to zero, the cut-off frequency is extremely large, while, for values of order equal to one, it is equal to the characteristic frequency ω_0.

Considering, for example, $\alpha = 0.3, 0.5, 0.7$, the values of the half-power frequency of a DO-LPF, calculated using (17), are summarized in Table 1. The corresponding values of the slope are provided in Table 2.

The corresponding values of the half-power frequency in the case of FO-LPFs of orders 0.3, 0.5, and 0.7 are 0.069 rad/s, 0.268 rad/s, and 0.533 rad/s, respectively. In the case of PL-LPFs the values are 3.013 rad/s, 1.732 rad/s, and 1.301 rad/s. The values of the associated slopes are −6 dB/dec, −10 dB/dec, and −14 dB/dec in both types of filters. Therefore, it is concluded that the cut-off frequency can be set using one of the orders of the filter and, at the same time, the slope can be adjusted by using the other order, whereas, in the FO-LPF and PL-LPF, the cut-off frequency and the slope are simultaneously determined by the order.

Table 1. Values of the half-power frequency of a DO-LPF with ω_0 = 1 rad/s.

	Cut-Off Frequency (rad/s)		
Order (β)	$\alpha = 0.3$	$\alpha = 0.5$	$\alpha = 0.7$
0.2	179.852	24.063	10.345
0.3	14.952	5.702	3.901
0.4	3.401	2.445	2.226
0.5	1.202	1.354	1.513
0.6	0.541	0.862	1.130
0.7	0.284	0.598	0.893
0.8	0.165	0.440	0.733
0.9	0.103	0.338	0.619
1	0.069	0.268	0.533

Table 2. Values of the slope of the transition between the pass-band and the stop-band of a DO-LPF.

	Slope (dB/dec)		
Order (β)	$\alpha = 0.3$	$\alpha = 0.5$	$\alpha = 0.7$
0.2	−1.2	−2.0	−2.8
0.3	−1.8	−3.0	−4.2
0.4	−2.4	−4.0	−5.6
0.5	−3.0	−5.0	−7.0
0.6	−3.6	−6.0	−8.4
0.7	−4.2	−7.0	−9.8
0.8	−4.8	−8.0	−11.2
0.9	−5.4	−9.0	−12.6
1	−6.0	−10.0	−14.0

2.2. High-Pass Filters

Considering the integer-order high-pass filter (HPF), which has a pole frequency ω_0 equal to the half-power frequency (ω_h), with a transfer function given by (19):

$$H_{HP}(s) = \frac{s}{s+\omega_0}\,. \tag{19}$$

Its gain and phase responses, obtained from (19) by setting $s = j\omega$, are given, respectively, by (20) and (21):

$$|H_{HP}(\omega)| = \frac{\frac{\omega}{\omega_0}}{\sqrt{\left(\frac{\omega}{\omega_0}\right)^2 + 1}}\,, \tag{20}$$

$$\angle H_{HP}(\omega) = \frac{\pi}{2} - \tan^{-1}\left(\frac{\omega}{\omega_0}\right). \tag{21}$$

The phase at this frequency becomes equal to $+\pi/4$, while the slope of the transition from the pass-band of the filter to the stop-band is equal to +20 dB/dec.

The fractional-order high-pass filter (FO-HPF) is described by the transfer function in (22):

$$H_{FOHP}(s) = \frac{s^\alpha}{s^\alpha + \omega_0^\alpha}\,, \tag{22}$$

and its magnitude and phase responses are

$$|H_{FOHP}(\omega)| = \frac{\left(\frac{\omega}{\omega_0}\right)^{\alpha}}{\sqrt{\left(\frac{\omega}{\omega_0}\right)^{2\alpha} + 2\left(\frac{\omega}{\omega_0}\right)^{\alpha}\cos(\frac{\alpha\pi}{2}) + 1}}, \tag{23}$$

$$\angle H_{FOHP}(\omega) = \frac{\alpha\pi}{2} - \tan^{-1}\left[\frac{\left(\frac{\omega}{\omega_o}\right)^{\alpha}\sin(\frac{\alpha\pi}{2})}{\left(\frac{\omega}{\omega_0}\right)^{\alpha}\cos(\frac{\alpha\pi}{2}) + 1}\right]. \tag{24}$$

Using (23) and (24), the half-power frequency, as well as the phase at this frequency, are given by (25) and (26):

$$\frac{\omega_{h,FOHP}}{\omega_0} = \left[\sqrt{1+\cos^2(\frac{\alpha\pi}{2})} + \cos(\frac{\alpha\pi}{2})\right]^{1/\alpha}, \tag{25}$$

$$\angle H_{FOHP}(\omega_{h,FOHP}) = \frac{\alpha\pi}{2} - \tan^{-1}\left[\frac{\sin(\frac{\alpha\pi}{2})}{2\cos(\frac{\alpha\pi}{2}) + \sqrt{1+\cos^2(\frac{\alpha\pi}{2})}}\right]. \tag{26}$$

The slope of the transition from the pass-band of the filter to the stop-band is $+20\cdot\alpha$ dB/dec.

The transfer function of the power-law high-pass filter (PL-HPF) is

$$H_{PLHP}(s) = \left(\frac{s}{s+\omega_0}\right)^{\beta}, \tag{27}$$

and the corresponding expressions are summarized in (28)–(31):

$$|H_{PLHP}(\omega)| = \frac{\left(\frac{\omega}{\omega_0}\right)^{\beta}}{\left[\left(\frac{\omega}{\omega_0}\right)^{2} + 1\right]^{\beta/2}}, \tag{28}$$

$$\angle H_{PLHP}(\omega) = \beta\cdot\left[\frac{\pi}{2} - \tan^{-1}\left(\frac{\omega}{\omega_0}\right)\right], \tag{29}$$

$$\frac{\omega_{h,PLHP}}{\omega_0} = \frac{1}{\sqrt{2^{1/\beta}-1}}, \tag{30}$$

$$\angle H_{PLHP}(\omega_{h,PLHP}) = \beta\cdot\left[\frac{\pi}{2} - \tan^{-1}\left(\frac{1}{\sqrt{2^{1/\beta}-1}}\right)\right]. \tag{31}$$

The distance between the half-power and pole frequencies is determined by the order of the filter; in addition, the gradient between the pass-band and the stop-band of the filter is equal to $+20\cdot\beta$ dB/dec.

Again, the main difference between the fractional-order and power-law filters concerns the relative position of the half-power frequencies ω_h with respect to the pole frequency ω_0. The results are the opposite ones to those derived in the case of the low-pass filters. In particular, for the fractional-order high-pass filter, the following condition applies: $\omega_{h,FOHP} > \omega_0$, while, for the power-law high-pass filter, $\omega_{h,PLHP} < \omega_0$ when $0 < \alpha, \beta < 1$. In both cases, as the order approaches one, the cut-off frequencies of the filters approach the characteristic frequency ω_0. This is demonstrated in the plots of Figure 2a, while the three-dimensional graph illustrating the relation of the cut-off frequency with the orders of the DO-HPF filter can be seen in Figure 2b.

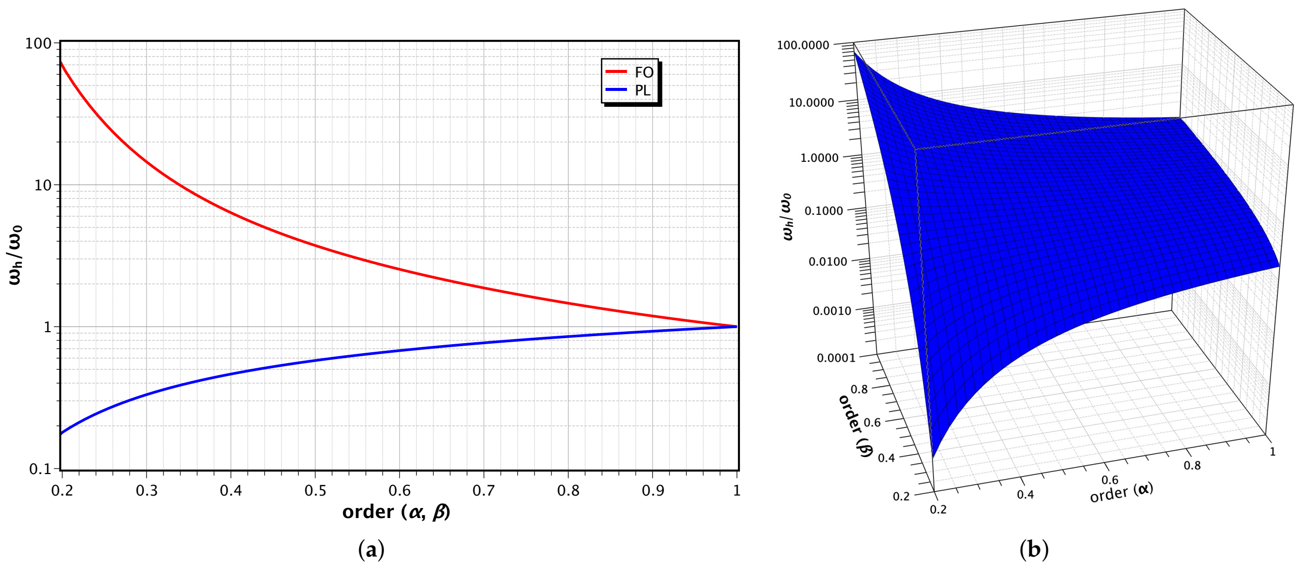

Figure 2. Variation in the half-power frequency of (**a**) FO-HPF and PL-HPF as a function of the order α, and (**b**) DO-HPF as a function of the orders (α, β).

3. Approximation of Non-Integer Order Filters

The approximation of the fractional-order transfer functions in (4) and (22) can be performed by utilizing the Oustaloup, Continued Fraction Expansion, etc. tools because they are based on the fractional Laplacian operator s^{α}. This is not possible in the cases of power-law and double-order transfer functions because of the existence of the power in the overall transfer function.

This can be overcome using the curve-fitting-based method also utilized in [15], and the resulting approximation transfer function has the form

$$H(s) = \frac{B_n s^n + B_{n-1} s^{n-1} + \ldots + B_1 s + B_0}{s^n + A_{n-1} s^{n-1} + \ldots + A_1 s + A_0}, \tag{32}$$

with A_i and B_j $(i = 0, 1, \ldots, n-1,\ j = 0, 1, \ldots, n)$ being positive and real coefficients, and n being the order of the approximation.

It must be mentioned at this point that the aforementioned approximation tool is also applicable in the case of the transfer functions in (4) and (22) and, consequently, the transfer function in (32) can be employed in all the cases of the filter presented in this work. Therefore, the double-order filter transfer function could be considered as the generalized form, where fractional-order and power-law filters are special cases with $\beta = 1$ and $\alpha = 1$, respectively.

Following this, and considering a fourth-order approximation in the range $[10^{-2}, 10^{+2}]$ rad/s, the coefficients of (32) in the case of the approximations of FO-LPF, FO-HPF (i.e., $\beta = 1$), PL-LPF, PL-HPF (i.e., $\alpha = 1$), and DO-LPF, DO-HPF with $(\alpha, \beta) = (0.7, 0.7)$ transfer functions are summarized in Table 3. Using the values in Table 3, the gain and phase responses, with their associated error plots, obtained using MATLAB, are demonstrated in Figures 3 and 4. The values of the approximated half-power frequencies and slopes, along with the corresponding theoretically predicted ones, are given in Table 4, confirming the accuracy of the employed approximation.

Table 3. Values of coefficients of (32) for realizing FO-LPFs and FO-HPFs of order equal to 0.7 (β = 1), PL-LPFs and PL-HPFs of order equal to 0.7 ($\alpha = 1$), and DO-LPF and DO-HPF of orders ($\alpha = 0.7$, β = 0.7).

Coefficient	FO-LPF	FO-HPF	PL-LPF	PL-HPF	DO-LPF	DO-HPF
A_0	1	1	697.3	0.001434	4.044	0.2473
A_1	15.36	15.36	1083	0.07309	49.47	6.332
A_2	34.23	34.23	455.9	0.6538	83.03	20.53
A_3	15.36	15.36	50.97	1.553	25.61	12.23
B_0	0.9792	0.02077	697.3	1.528×10^{-5}	3.979	0.01685
B_1	12.58	2.786	595.2	0.005866	42.05	1.696
B_2	17.11	17.11	112	0.1607	47.48	11.74
B_3	2.786	12.58	4.09	0.8536	6.858	10.4
B_4	0.02077	0.9792	0.01066	1	0.06816	0.9838

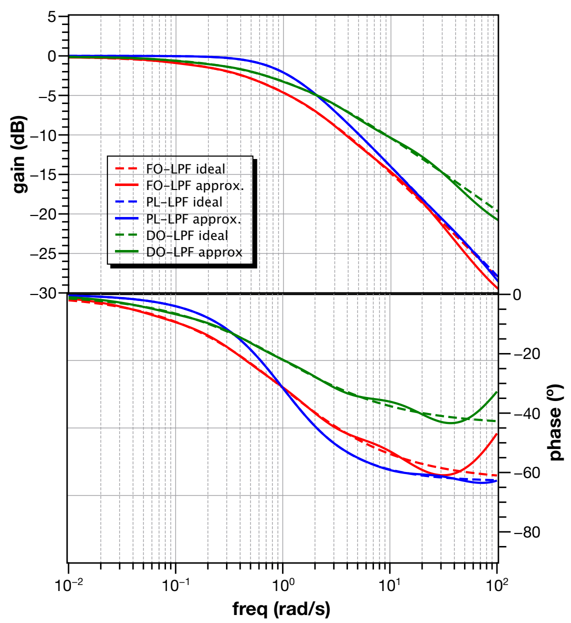

(**a**)

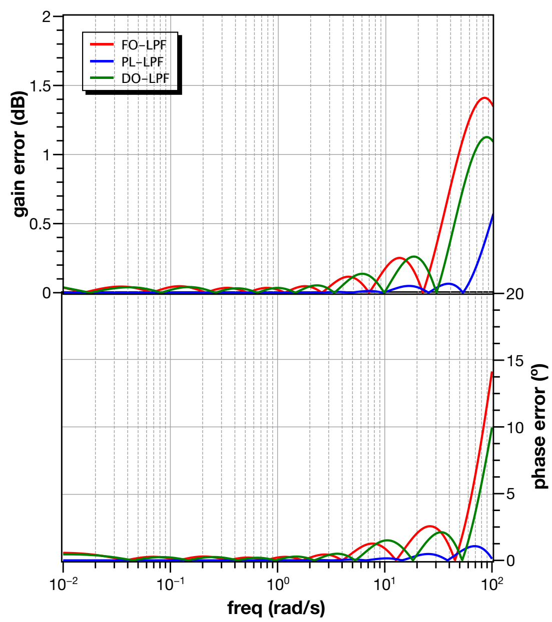

(**b**)

Figure 3. (**a**) Gain and phase responses of the LPFs derived from (32) for (α, β) = (0.7, 1), (1, 0.7), (0.7, 0.7), and (**b**) their associated error plots.

Table 4. Values of the half-power frequencies and slopes obtained from the plots in Figures 3 and 4.

Type of Filter	Half-Power Frequency (rad/s)		Slope (dB/dec)	
	Approximated	Theoretical	Approximated	Theoretical
FO-LPF (α, β) = (0.7, 1)	0.532	0.533	−13.95	−14
PL-LPF (α, β) = (1, 0.7)	1.305	1.301	−14.1	−14
DO-LPF (α, β) = (0.7, 0.7)	0.895	0.893	−9.5	−9.8
FO-HPF (α, β) = (0.7, 1)	1.731	1.747	13.9	14
PL-HPF (α, β) = (1, 0.7)	0.7689	0.7689	14.2	14
DO-HPF (α, β) = (0.7, 0.7)	1.062	1.062	10.2	9.8

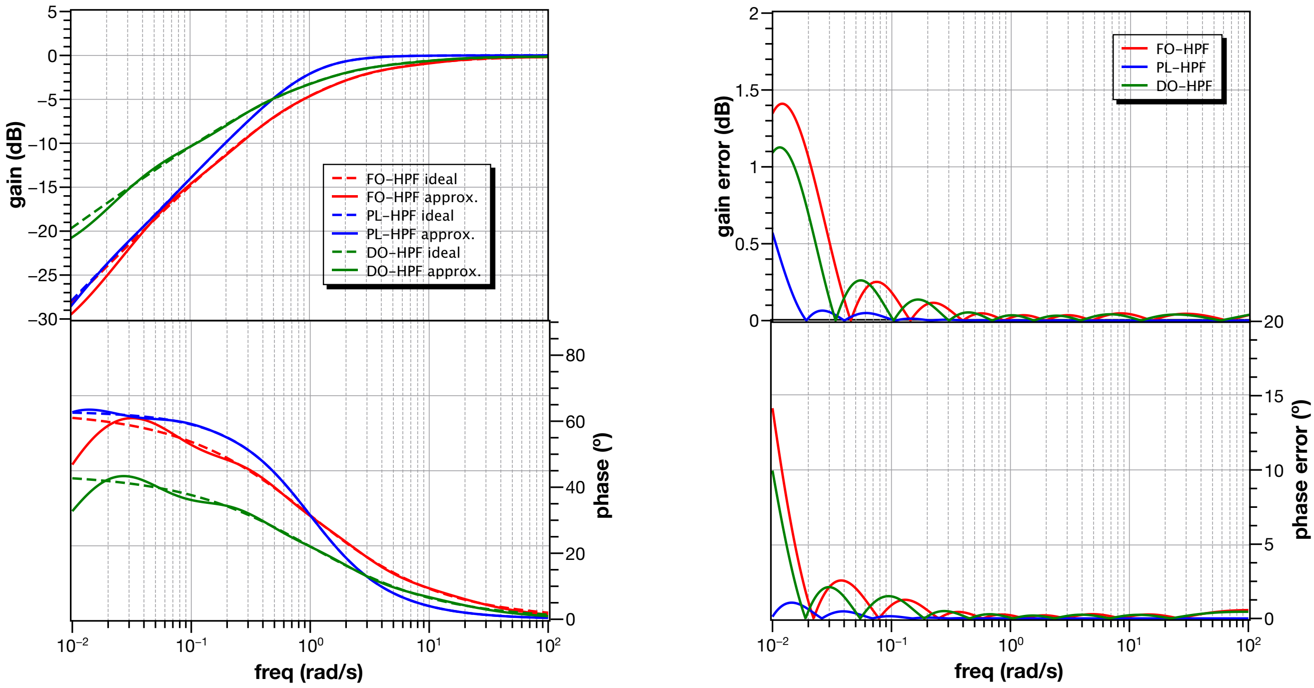

(**a**) (**b**)

Figure 4. (**a**) Gain and phase responses of the HPFs derived from (32) for (α, β) = (0.7, 1), (1, 0.7), (0.7, 0.7), and (**b**) their associated error plots.

A possible implementation of the transfer function in (32) could be performed using the functional block diagram in Figure 5, where the realized transfer function is

$$H(s) = \frac{G_4 s^4 + \frac{G_3}{\tau_1} s^3 + \frac{G_2}{\tau_1 \tau_2} s^2 + \frac{G_1}{\tau_1 \tau_2 \tau_3} s + \frac{G_0}{\tau_1 \tau_2 \tau_3 \tau_4}}{s^4 + \frac{1}{\tau_1} s^3 + \frac{1}{\tau_1 \tau_2} s^2 + \frac{1}{\tau_1 \tau_2 \tau_3} s + \frac{1}{\tau_1 \tau_2 \tau_3 \tau_4}} . \tag{33}$$

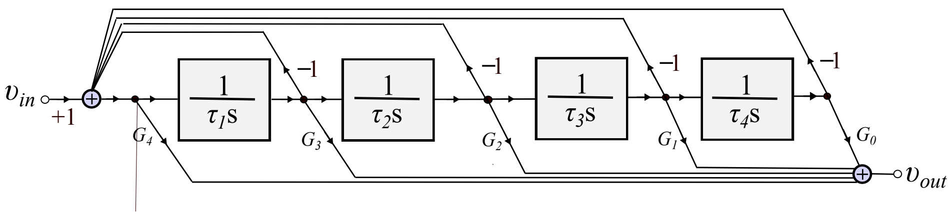

Figure 5. Follow -the-Leader Feedback (FLF) structure for implementing the rational integer-order function in (32).

Equalizing the coefficients of (32) and (33), the resulting design equations are given by (34):

$$\tau_{i+1} = \frac{A_{4-i}}{A_{3-i}} \, (i = 0 \ldots 3) \qquad G_j = \frac{B_j}{A_j} \, (j = 0 \ldots 4) \, . \tag{34}$$

Assuming that ω_0 = 1 rad/s, then, using the design equations in (34) and the data in Table 3, the resulting values of time constants and scaling factors are provided in Table 5.

Table 5. Values of time-constants and scaling factors of (33) for realizing FO-LPF and FO-HPF of order equal to 0.7 ($\beta = 1$), PL-LPF and PL-HPF of order equal to 0.7 ($\alpha = 1$), and DO-LPF and DO-HPF of orders equal to (0.7, 0.7) .

Coefficient	FO-LPF	FO-HPF	PL-LPF	PL-HPF	DO-LPF	DO-HPF
τ_1	65.090 ms	65.090 ms	19.621 ms	643.723 ms	39.050 ms	81.751 ms
τ_2	448.886 ms	448.886 ms	111.803 ms	2.376 s	308.433 ms	595.848 ms
τ_3	2.228 s	2.228 s	420.848 ms	8.944 s	1.678 s	3.242 s
τ_4	15.363 s	15.363 s	1.554	50.966 s	12.232 s	25.608 s
G_0	0.979	0.021	1	0.011	0.984	0.068
G_1	0.819	0.181	0.550	0.080	0.850	0.268
G_2	0.5	0.5	0.246	0.246	0.572	0.572
G_3	0.181	0.819	0.080	0.550	0.268	0.850
G_4	0.021	0.979	0.011	1	0.068	0.984

To conclude, the design steps that must be followed for implementing the filter functions are as follows:

Step#1: Choice of the suitable transfer function (order(s) and pole frequency), to fulfill the given specifications of the filter;
Step#2: Employment of the curve-fitting-based technique presented in detail in [15], to obtain the approximation transfer function which has the form shown in (32);
Step#3: Employment of the design equations in (34), to obtain the values of time constants and scaling factors;
Step#4: Realization of the required integration, summation, and scaling operations, using suitable active elements/stages.

4. Experimental Results

The presented generalized structure was verified using an Anadigm FPAA AN231E04 device [16,17]. Using the *Anadigm Designer*$^{®}$*2* EDA software, the resulting design is depicted in Figure 6. The frequency responses of the LPFs are demonstrated in Figure 7a. The measured values of the cut-off frequencies were 2.606 krad/s for the FO-LPF, 6.826 krad/s for the PL-LPF, and 4.427 krad/s for the DO-LPF, with the corresponding theoretical values being 2.668 krad/s, 6.503 krad/s, and 4.464 krad/s, respectively. In the case of the HPFs, the measurements were 8.804 krad/s, 3.887 krad/s, and 5.313 krad/s, with the values predicted by theory being 9.37 krad/s, 3.844 krad/s, and 5.6 krad/s.

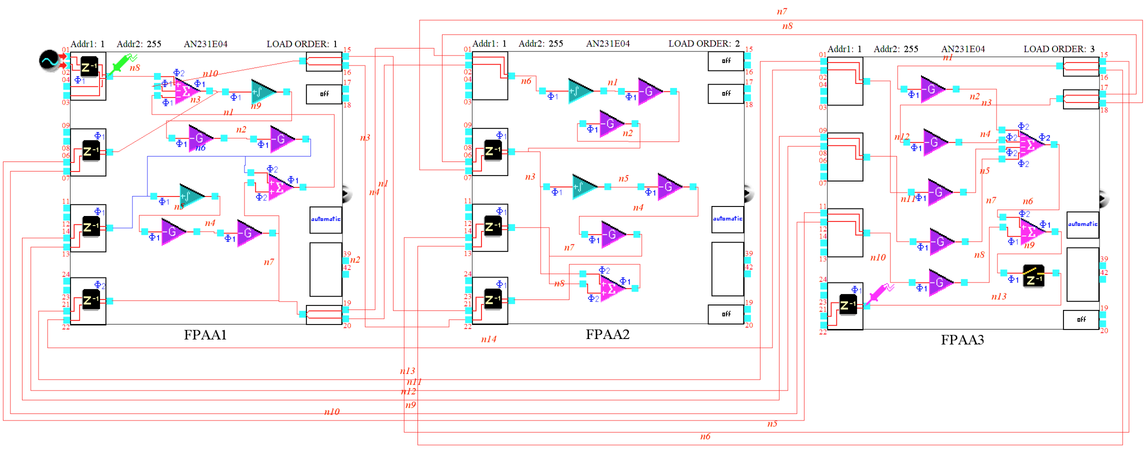

Figure 6. FPAA configuration for realizing FO, PL, and DO-LPFs and -HPFs.

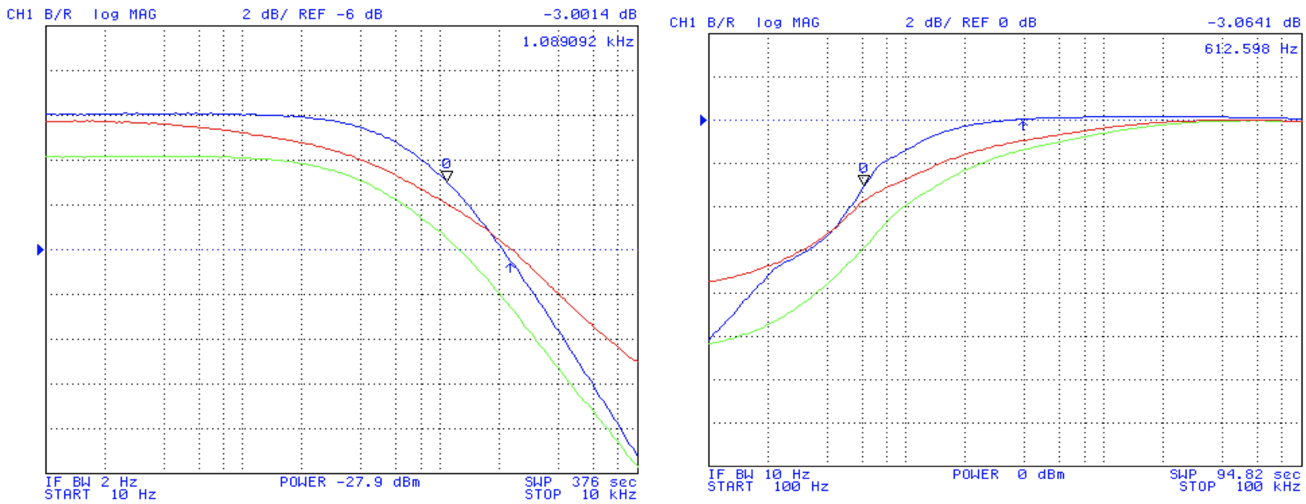

(**a**) (**b**)

Figure 7. Experimental frequency responses of the (**a**) FO (green), PL (red), and DO (blue) low-pass filters, and (**b**) FO (green), PL (red), and DO (blue) high-pass filters.

The time-domain behavior of the filters was evaluated by stimulating the DO-LPF and DO-HPFs of orders (α, β) equal to (0.7, 0.7). For this purpose, a 600 mVp–p sinusoidal signal with frequency equal to the cut-off frequency was used, and the obtained waveforms are demonstrated in Figure 8a,b. The values of the corresponding gains were -2.94 dB and -2.84 dB, while the values of the phase differences between the output and the input of the filters was $-18°$, $17°$, close to the theoretically predicted ones of $-21°$, $21.5°$.

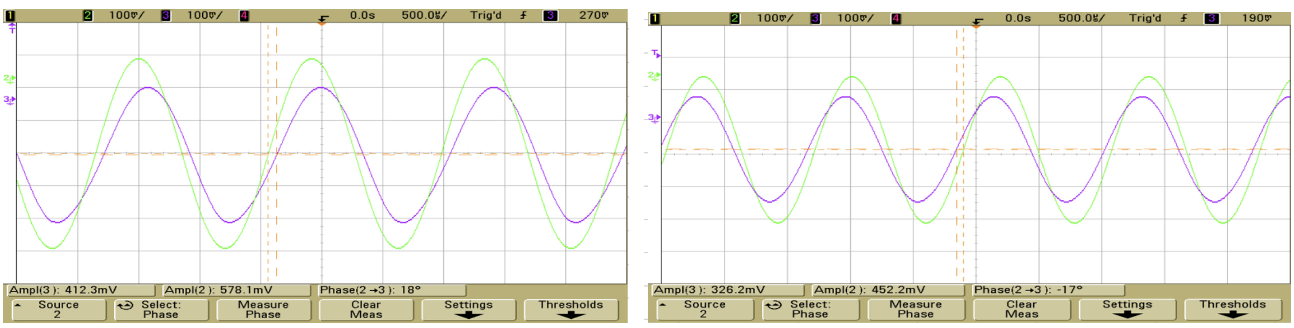

(**a**) (**b**)

Figure 8. Experimental input and output waveforms of (**a**) DO-LPF and (**b**) DO-HPF of orders (α, β) equal to (0.7, 0.7).

5. Conclusions

A generalized programmable structure with the capability of implementing non-integer-order LPFs and HPFs, with orders in the range (0, 1), is introduced in this work. The performed comparison shows that FO filters have the opposite effect in the half-power frequency to that caused by the PL filters. Their enhanced version, named DO filters, is versatile, in the sense that it could be programmed to offer the desired scaling of the half-power frequency, according to the imposed specifications. In addition, due to the extra degrees of freedom that are offered, the slope of the gradient between the pass-band and the stop-band of the filter can be further adjusted, instead of being pre-determined by the order of the filter, as happens in the case of FO and PL filters. The provided experimental results, obtained using an FPAA device, confirm that the design offers flexibility and versatility, and confirm the validity of the presented analysis.

Author Contributions: Conceptualization, C.P., A.P. and A.S.E.; methodology, A.P. and C.P.; software, A.P.; validation, A.P.; formal analysis, A.P.; investigation, A.P. and C.P.; writing—original draft preparation, C.P.; writing—review and editing, C.P. and A.S.E.; project administration, C.P. and A.S.E. All authors have read and agreed to the published version of the manuscript.

Funding: This research received no external funding.

Data Availability Statement: No new data were created or analyzed in this study. Data sharing is not applicable to this article.

Conflicts of Interest: The authors declare no conflict of interest.

Abbreviations

The following abbreviations are used in this manuscript:

DO	Double-Order
DO-HPF	Double-Order High-Pass Filter
DO-LPF	Double-Order Low-Pass Filter
FPAA	Field Programmable Analog Array
FO	Fractional-Order
FO-HPF	Fractional-Order High-Pass Filter
FO-LPF	Fractional-Order Low-Pass Filter
FLF	Follow-the-Leader Feedback
HPF	High-Pass Filter
LPF	Low-Pass Filter
Op-Amp	Operational Amplifier

References

1. Tsirimokou, G.; Psychalinos, C.; Elwakil, A. *Design of CMOS Analog Integrated Fractional-Order Circuits: Applications in Medicine and Biology*; Springer: Berlin/Heidelberg, Germany, 2017. [CrossRef]
2. Adhikary, A.; Sen, S.; Biswas, K. Practical realization of tunable fractional order parallel resonator and fractional order filters. *IEEE Trans. Circuits Syst. I Regul. Pap.* **2016**, *63*, 1142–1151. [CrossRef]
3. Dvorak, J.; Langhammer, L.; Jerabek, J.; Koton, J.; Sotner, R.; Polak, J. Synthesis and analysis of electronically adjustable fractional-order low-pass filter. *J. Circuits Syst. Comput.* **2018**, *27*, 1850032. [CrossRef]
4. Jerabek, J.; Sotner, R.; Dvorak, J.; Polak, J.; Kubanek, D.; Herencsar, N.; Koton, J. Reconfigurable fractional-order filter with electronically controllable slope of attenuation, pole frequency and type of approximation. *J. Circuits Syst. Comput.* **2017**, *26*, 1750157. [CrossRef]
5. Khalil, N.A.; Said, L.A.; Radwan, A.G.; Soliman, A.M. Generalized two-port network based fractional order filters. *AEU-Int. J. Electron. Commun.* **2019**, *104*, 128–146. [CrossRef]
6. Kostelac, F.; Ćoza, A.; Jurišić, D. Fractional-Order Elements Using Tunable OTA-C Structures. In Proceedings of the 2021 44th International Convention on Information, Communication and Electronic Technology (MIPRO), Opatija, Croatia, 27 September–1 October 2021; pp. 119–124. [CrossRef]
7. Langhammer, L.; Dvorak, J.; Sotner, R.; Jerabek, J.; Bertsias, P. Reconnection–less reconfigurable low–pass filtering topology suitable for higher–order fractional–order design. *J. Adv. Res.* **2020**, *25*, 257–274. [CrossRef] [PubMed]
8. Mahata, S.; Herencsar, N.; Kubanek, D. On the design of power law filters and their inverse counterparts. *Fractal Fract.* **2021**, *5*, 197. [CrossRef]
9. Mohapatra, A.S.; Biswas, K. A fractional order notch filter to compensate the attenuation-loss due to change in order of the circuit. *IEEE Trans. Circuits Syst. I Regul. Pap.* **2020**, *68*, 655–666. [CrossRef]
10. Freeborn, T.J.; Maundy, B.; Elwakil, A.S. Field programmable analogue array implementation of fractional step filters. *IET Circuits Devices Syst.* **2010**, *4*, 514–524. [CrossRef]
11. Kapoulea, S.; Psychalinos, C.; Elwakil, A.S. Versatile Field-Programmable Analog Array realizations of power-law filters. *Electronics* **2022**, *11*, 692. [CrossRef]
12. Kapoulea, S.; Psychalinos, C.; Elwakil, A.S. Double exponent fractional-order filters: Approximation methods and realization. *Circuits Syst. Signal Process.* **2021**, *40*, 993–1004. [CrossRef]
13. Tsirimokou, G.; Psychalinos, C.; Elwakil, A.S. Fractional-order electronically controlled generalized filters. *Int. J. Circuit Theory Appl.* **2017**, *45*, 595–612. [CrossRef]
14. Tsouvalas, E.; Kapoulea, S.; Psychalinos, C.; Elwakil, A.S.; Jurišić, D. Electronically controlled power-law filters realizations. *Fractal Fract.* **2022**, *6*, 111. [CrossRef]
15. Kapoulea, S.; Psychalinos, C.; Elwakil, A.S. Power law filters: A new class of fractional-order filters without a fractional-order Laplacian operator. *AEU-Int. J. Electron. Commun.* **2021**, *129*, 153537. [CrossRef]

16. Anadigm. AN231E04 dpASP: The AN231E04 dpASP Dynamically Reconfigurable Analog Signal Processor. Available online: https://anadigm.com/an231e04.asp (accessed on 4 April 2023).
17. Tlelo-Cuautle, E.; Pano-Azucena, A.D.; Guillén-Fernández, O.; Silva-Juárez, A. *Analog/Digital Implementation of Fractional Order Chaotic Circuits and Applications*; Springer: Berlin/Heidelberg, Germany, 2020. [CrossRef]